Anisotropic self-diffusion in colloidal nematic phases

Hartmut Löwen
Institut für Theoretische Physik II, Heinrich-Heine-Universität Düsseldorf, Universitätsstraße 1, D-40225 Düsseldorf, Germany
and Institut für Festkörperforschung, Forschungszentrum Jülich, D-52425 Jülich, Germany
(Received 8 September 1998)

By computer simulation the anisotropic long-time translational self-diffusion coefficients are calculated in the nematic phase of colloidal hard spherocylinders exhibiting Brownian dynamics in a solvent. In particular, the two diffusion coefficients $D_L^{\parallel}$ and $D_L^{\perp}$, parallel and perpendicular to the nematic director, are obtained for aspect ratios between 4.8 and 16 and for arbitrary densities. Long-time diffusion along the nematic director is nonmonotonic in density: Upon increasing the density, it first increases due to stronger alignment and then decreases due to packing constraints. It is shown that the ratio $D_L^{\parallel}/D_L^{\perp}$ and the orientation flip rate essentially scale with the nematic order parameter. While the ratio $D_L^{\parallel}/D_L^{\perp}$ increases with density in the nematic phase, it decreases dramatically with increasing density in the smectic-*A* phase. The results are compared to recent experiments. [S1063-651X(99)03602-8]

PACS number(s): 82.70.−y, 61.30.−v, 66.10.−x

I. INTRODUCTION

Since the pioneering work of Onsager [1], it has been known that a system of hard spherocylinders undergoes a first-order transition from an isotropic phase to a nematic phase provided the aspect ratio is sufficiently high. While both the translational and orientational degrees of freedom of the rods are completely disordered in the isotropic (or fluid) phase, there is a macroscopic director along which the rod orientations are ordered in the nematic phase but the center-of-mass positions of the rods are still disordered. Most of the recent theoretical and computer simulation work [2] has focused on structural correlations [3] and on the location of the isotropic-nematic transition for hard rods [4–10] as well as for charged and flexible particles [11–16]. On the other hand, detailed experimental data are available tracing the phase boundaries for different rodlike colloidal samples [17–19].

While there is an increasing understanding of the static and thermodynamic properties of rodlike particles, it is fair to say that *dynamical* correlations are far less studied. For colloidal samples, the dynamics are Brownian rather than Newtonian as for molecular liquid crystals [20–22]. A tremendous difficulty in the theoretical description of the Brownian case concerns the long-ranged hydrodynamic interactions mediated by the solvent flow. These interactions can, however, be neglected for low volume fractions of the colloidal particles. Correspondingly, in most of the recent Brownian dynamics simulations, the long-time self-diffusion coefficients for strongly interacting particles were calculated neglecting hydrodynamic interactions. Results were obtained both for spherical particles (see, e.g., Refs. [23–30]), as well as for anisotropic particles modeled by hard rods [31] and by two- [32,33] and many- [34–36] site-models. On the other hand, experiments using fluorescence recovery after photobleaching (FRAP) for boehmite rods [37,38] and Pyridin [39] were performed, and good overall agreement was obtained between the experimental data of van Bruggen, Lekkerkerker, and Dhont [37] with the results of Brownian dynamics computer simulation for hard spherocylinders [31].

With the exception of Ref. [36], all these previous studies were performed in the isotropic phase. In the present work we extend these investigations exploring the dynamical correlations systematically over a broad stability range of the *nematic* phase and we also include results for the smectic-*A* phase. As in Ref. [31], we use a hard spherocylinder model with excluded volume interactions. The reason for doing so is twofold: First, this model is governed by two parameters only, namely, the aspect ratio and the rod number density. Second, the stability range of the nematic phase is known precisely by recent computer simulations of Bolhuis and Frenkel [9]. Clearly, in the nematic phase, the long-time mean-square displacement becomes *anisotropic*, i.e., it can be split into parts parallel and perpendicular to the nematic director. Consequently there are two long-time self-diffusion coefficients $D_L^{\parallel}$ and $D_L^{\perp}$. In the present study we calculate them both over a large stability range of the nematic phase, including cylinder aspect ratios ranging between 4.8 and 16. We find a nonmonotonic behavior of $D_L^{\parallel}$ for increasing density, and show that the ratio $D_L^{\parallel}/D_L^{\perp}$ and the orientation flip rate essentially depend on the nematic order parameter alone. This ratio $D_L^{\parallel}/D_L^{\perp}$ is found to increase with density in the nematic phase, and to decrease with density in the smectic-*A* phase.

Our study is also motivated by recent pioneering FRAP experiments of van Bruggen *et al.* [40], where the dynamics perpendicular and parallel to the nematic director were resolved and distinguished in the nematic phase of boehmite rods. It was found that the diffusion coefficients are mainly dominated by the density, and are comparable to that extrapolated from the isotropic phase. It was further found that the ratio of the two long-time diffusion coefficients $D_L^{\parallel}$ and $D_L^{\perp}$, parallel and perpendicular to the nematic director, is at about 2–3 at the nematic density coexisting with the isotropic phase. In our Brownian dynamics simulations we confirm these findings.

The paper is organized as follows: In Secs. II and III, we discuss the model and the Brownian dynamics algorithm. Results for the different diffusion coefficients are given and

discussed in Sec. IV. Finally we conclude in Sec. V.

II. MODEL

The model and its Brownian dynamics is similar to that studied previously in Ref. [31]: N spherocylinders with total width L and diameter σ are in a volume V; their aspect ratio is $p=L/\sigma$ [41]. A rod configuration is characterized by its center-of-mass coordinates $\{\vec{R}_i \equiv (X_i, Y_i, Z_i), i=1, \ldots, N\}$ and orientations $\{\vec{\Omega}_i, i=1, \ldots, N\}$, where $\vec{\Omega}_i$ is a unit vector. The potential energy is zero if the rods do not overlap and infinite else. Consequently the temperature T simply sets the energy scale and the rod number density $\rho=N/V$ is the only relevant thermodynamic variable which is conveniently expressed in terms of the rod packing fraction

$$\eta=\rho\pi\sigma^2(\sigma/6+(L-\sigma)/4). \tag{1}$$

The bulk phase diagram only depends on η and p. Henceforth we choose the rod diameter σ as a suitable unit of length.

Neglecting hydrodynamic interactions, the short-time Brownian dynamics of the rods is characterized by two translational short-time diffusion constants $D^{\perp}$ and $D^{\parallel}$, perpendicular and parallel to the rod axis, and a rotational short-time diffusion constant D^r. For a single cylinder in a solvent, these three diffusion constants have been calculated as a function of p by Broersma [42] and Tirado and co-workers [43,44]. We have used the analytical expressions proposed by in Ref. [44]:

$$D^{\perp}=\frac{D_0}{4\pi}(\ln p+0.839+0.185/p+0.233/p^2), \tag{2}$$

$$D^{\parallel}=\frac{D_0}{2\pi}(\ln p-0.207+0.980/p-0.133/p^2), \tag{3}$$

$$D^{r}=\frac{3D_0}{\pi L^2}(\ln p-0.662+0.917/p-0.050/p^2), \tag{4}$$

with

$$D_0=k_BT/\eta_sL, \tag{5}$$

where k_B is Boltzmann's constant and η_s the shear viscosity of the solvent. Our basic time scale is

$$\tau=\sigma^2/D_0. \tag{6}$$

Since we neglected hydrodynamic interactions, our model does not describe the correct dynamics of hard spherocylinders at high packing fractions. Nevertheless the model can still be used if a soft interaction between the rods is present (as e.g., for charged rods) which can be mapped onto *effective* hard spherocylinders [45,15,6]. In this case, one has to distinguish between the effective packing fraction resulting from the interactions and the physical packing fraction of the rods. Typically, the physical packing fraction is much smaller than the effective packing fraction. Since the hydrodynamic interactions are governed by the physical packing fraction, one can still safely neglect them. However, there is still an inconsistency of the model since we assumed in the Eqs. (2)–(4) that the effective aspect ratio stemming from the effective interactions and the physical aspect ratio are the same. This inconsistency is not severe, since the p dependence in Eqs. (2)–(4) is weak. In fact, our model was successfully used to describe self-diffusion data for silica coated boehmite rods in the isotropic phase [37].

III. BROWNIAN DYNAMICS SIMULATIONS

We use a sequential Brownian dynamics scheme. A sufficiently small time step Δt is used, and a nonoverlapping starting configuration is given. In one elementary trial step of the simulation, one rod which is labeled by i in the following is chosen randomly and a translational and rotational trial move is made. First, the center-of-mass coordinate $\vec{R}_i$ of the ith rod is moved. It can be composed into a part parallel $\vec{R}_i^{\parallel} \equiv (\vec{\Omega}_i \cdot \vec{R}_i)\vec{\Omega}_i$ to the orientation $\vec{\Omega}_i$, and another part $\vec{R}_i^{\perp}$ perpendicular to $\vec{\Omega}_i$, such that $\vec{R}_i=\vec{R}_i^{\parallel}+\vec{R}_i^{\perp}$. Within the move, the parallel part $\vec{R}_i^{\parallel}$ is replaced by $\vec{R}_i^{\parallel}+(\Delta R^{\parallel})\vec{\Omega}_i$, and the perpendicular part $\vec{R}_i^{\perp}$ is replaced by $\vec{R}_i^{\perp}+(\Delta R_1^{\perp})\vec{e}_{i1}+(\Delta R_2^{\perp})\vec{e}_{i2}$. Here $(\Delta R^{\parallel})$ is a Gaussian distributed random number with zero mean and variance $2D^{\parallel}\Delta t$, while $(\Delta R_1^{\perp})$ and $(\Delta R_2^{\perp})$ are both Gaussian random numbers with zero mean and variance $2D^{\perp}\Delta t$. Furthermore, $\vec{e}_{i1}$ and $\vec{e}_{i2}$ are two orthogonal unit vectors perpendicular to $\vec{\Omega}_i$. If the new rod configuration is free of overlaps, it is accepted, otherwise it is discarded. Next $\vec{\Omega}_i$ is replaced by $\vec{\Omega}_i+x_1\vec{e}_{i1}(t)+x_2\vec{e}_{i2}(t)$, where now x_1 and x_2 are Gaussian random numbers with zero mean and variance $2D^r\Delta t$. The new orientation vector is scaled appropriately to have unit length. Again, if this move leads to no rod overlap, it is accepted, otherwise it is rejected. After N_e elementary trial steps the corresponding physical time is $t=N_e\Delta t/N$. This sequential algorithm corresponds to real Brownian dynamics only if Δt is sufficiently small. Then one is able to generate ''toothed'' trajectories $\{\vec{R}_i(t), \vec{\Omega}_i(t)\}$ of the rods. The smallness of Δt is the real bottleneck of the simulation; typically we use $\Delta t/\tau=O(10^{-4})$. Therefore a huge number of elementary trial steps (typically 10^8) are required in order to obtain correct statistical averages for long-time properties. The same methods as given in Ref. [31] were used to check that the results were insensitive to a further reduction of the time step. The aspect ratio p was varied between 4.8 and 16. With two exceptions where the smectic-A phase was explored, the packing fraction was always in the stability range of the nematic phase. All parameters of the runs are summarized in Table I.

A rectangular simulation box with a square base and periodic boundary conditions is used. The box length in the x and y directions is L_0, while it is χL_0 in the z direction, with $\chi>1$ measuring the anisotropy of the cell. Consequently, $L_0=(N/\chi\rho)^{1/3}$. For the actual numbers, see Table I. The starting configuration was completely aligned along the z direction, and was put on a body-centered-tetragonal lattice as far as the rod positions are concerned. The director $\vec{\Omega}_0$ of the nematic phase was always very close to the z direction. Therefore, the anisotropic box minimizes finite-size effects in the nematic phase [9]. During the simulation the center-of-mass coordinate of the whole system was fixed in order to

TABLE I. Parameters of the different runs. Given are the rod packing fraction η, the aspect ratio p, the number N of rods in the simulation box, the time step Δt, the total time T over which statistics was taken, the maximal time t_m of the time window where dynamical correlations were explored, and the anisotropy χ of the simulation box. The time unit is $\tau=\sigma^2/D_0$.

η	p	N	$\Delta t/\tau$	T/τ	t_m/τ	χ
0.48	4.8	432	0.0002	180.0	100.0	4.0
0.41	6.0	432	0.0002	20.0	20.0	4.5
0.453	6.0	432	0.0002	60.0	30.0	4.6
0.28	10.0	486	0.0005	40.0	25.0	3.0
0.3	10.0	432	0.0005	50.0	25.0	3.0
0.35	10.0	432	0.0005	60.0	25.0	7.0
0.4	10.0	432	0.0003	20.0	20.0	7.0
0.44	10.0	432	0.0003	30.0	20.0	7.0
0.46	10.0	392	0.001	200.0	100.0	10.5
0.50	10.0	392	0.001	200.0	100.0	11
0.21	16.0	486	0.0005	60.0	25.0	3.8
0.23	16.0	432	0.0005	60.0	25.0	8.0
0.25	16.0	432	0.0005	125.0	25.0	8.0
0.3	16.0	432	0.0004	60.0	24.0	8.0
0.35	16.0	432	0.0004	30.0	24.0	8.0
0.4	16.0	400	0.0003	40.0	24.0	10.0
0.44	16.0	486	0.0005	40.0	25.0	3.8

avoid spurious diffusion of the whole system.

In order to check equilibration and to identify the different liquid-crystalline phases correctly, we have monitored nematic and smectic order parameters. The nematic order parameter S and the direction of the nematic director $\vec{\Omega}_0$ were obtained as the largest eigenvalue and the corresponding unit eigenvector of the second-rank tensor

$$\mathbf{Q}=\frac{1}{N}\sum_{i=1}^{N}\frac{3}{2}\langle\vec{\Omega}_i\otimes\vec{\Omega}_i\rangle-\frac{1}{2}\mathbf{1}. \tag{7}$$

Here $\otimes$ denotes the dyadic product, $\mathbf{1}$ is the unit second-rank tensor, and $\langle\cdots\rangle$ is a canonical average. Note that $\vec{\Omega}_0$ is only defined up to a sign. A set of smectic order parameters $\{\zeta_n\}$, on the other hand, can be defined as

$$\zeta_n=\frac{1}{N}\sum_{i=1}^{N}\langle\cos(2\pi n Z_i/\chi L_0)\rangle, \tag{8}$$

measuring smectic ordering along the z axis. Here Z_i denotes the z coordinate of the center of mass of the ith rod. A nematic phase can clearly be detected if $S\neq 0$ and $\zeta_n=0$ for any integer n. On the other hand, in a smectic-A phase, $S\neq 0$ and $\zeta_n\neq 0$, and there is no long-range ordering in the xy plane.

IV. TRANSLATIONAL LONG-TIME SELF-DIFFUSION

A. Definition of the quantities

The long-time self-diffusion splits into two parts; one of them, $D_L^{\parallel}$, is parallel to the nematic director $\vec{\Omega}_0$, while the other, $D_L^{\perp}$, is perpendicular to $\vec{\Omega}_0$. In detail, the definition of $D_L^{\parallel}$ is

$$D_L^{\parallel}=\lim_{t\to\infty}D^{\parallel}(t), \tag{9}$$

with

$$D^{\parallel}(t)=W^{\parallel}(t)/2t, \tag{10}$$

where

$$W^{\parallel}(t)=\frac{1}{N}\sum_{i=1}^{N}\langle[\vec{\Omega}_0\cdot(\vec{R}_i(t)-\vec{R}_i(0))]^2\rangle \tag{11}$$

is the mean square displacement of the center-of-mass coordinate parallel to the nematic director. Similarly, let us define

$$D_L^{\perp}=\lim_{t\to\infty}D^{\perp}(t), \tag{12}$$

with

$$D^{\perp}(t)=W^{\perp}(t)/4t, \tag{13}$$

where

$$W^{\perp}(t)=\frac{1}{N}\sum_{i=1}^{N}\langle\{(\vec{R}_i(t)-\vec{R}_i(0))-\vec{\Omega}_0[\vec{\Omega}_0\cdot(\vec{R}_i(t)-\vec{R}_i(0))]\}^2\rangle. \tag{14}$$

By splitting the different terms in the square of Eqs. (11) and (14), it is possible to calculate both $\vec{\Omega}_0$ and $W^{\parallel}(t)$ $[W^{\perp}(t)]$ during the run.

Alternatively one can define

$$D_L^{\parallel}=\lim_{t\to\infty}\frac{1}{2}\frac{d}{dt}W^{\parallel}(t) \tag{15}$$

and

$$D_L^{\perp}=\lim_{t\to\infty}\frac{1}{4}\frac{d}{dt}W^{\perp}(t). \tag{16}$$

The latter formula has the advantage of quicker convergence as $t\to\infty$, although the statistical error is larger since it is a differential quantity. By comparing both expressions during the simulation, we checked whether the infinite-time limit has been reached, and extracted an error in the data. In every case, both, $D^{\perp}(t)$ and $D^{\parallel}(t)$ were monotonically decreasing in time, which seems to be an expected formal property of Brownian rod systems (as in the case of Brownian spheres). In general, it was observed that the convergence of $D^{\perp}(t)$ to its infinite-time limit $D_L^{\perp}$ is faster than that of $D^{\parallel}(t)$. Henceforth we use $D^{\parallel}$ and $D^{\perp}$ as natural scales for $D_L^{\parallel}$ and $D_L^{\perp}$, respectively.

B. Results for $D_L^{\parallel}$ and $D_L^{\perp}$ in the nematic phase

Results for the long-time self-diffusion coefficients are summarized in Table II. For $p=6$, 10, and 16, we have also graphically displayed these results in Fig. 1–3. Defining an ''isotropized'' value of the long-time self-diffusion by $D_L^{(\mathrm{iso})}=(2D\perp_L+D_L^{\parallel})/3$, it is tempting to compare $D_L^{(\mathrm{iso})}$ with

TABLE II. Results of the different runs. Given are the rod packing fraction η, the length to width ratio p; the nematic order parameter S; the ratios $D_L^{\parallel}/D^{\parallel}$, $D_L^{\perp}/D^{\perp}$, $D_L^{\parallel}/D_L^{\perp}$, and $D_L^{(\mathrm{iso})}/D^t$; and the logarithm of the reduced orientation flip rate $\Gamma\tau$ per particle. The number in brackets gives an estimate for the error of the last digit. The two runs with $p=10$ and $\eta=0.46$ and 0.50 are in the smectic-A phase.

η	p	S	$D_L^{\parallel}/D^{\parallel}$	$D_L^{\perp}/D^{\perp}$	$D_L^{\parallel}/D_L^{\perp}$	$D_L^{(\mathrm{iso})}/D^t$	$\ln\Gamma\tau$
0.48	4.8	0.55(1)	0.13(1)	0.08(1)	2.1(1)	0.10(1)	−7.5
0.41	6	0.48(1)	0.22(1)	0.12(1)	2.4(1)	0.16(1)	−6.2
0.43	6	0.71(1)	0.24(2)	0.10(1)	3.1(2)	0.16(1)	−8.6
0.453	6	0.75(1)	0.20(1)	0.09(1)	3.0(1)	0.13(1)	−8.8
0.28	10	0.68(1)	0.51(2)	0.21(1)	3.3(2)	0.30(1)	−8.2
0.3	10	0.76(1)	0.54(1)	0.16(1)	4.7(2)	0.31(1)	−8.6
0.35	10	0.88(1)	0.59(2)	0.14(1)	5.8(2)	0.32(1)	-
0.4	10	0.943(7)	0.52(1)	0.11(1)	6.5(2)	0.28(1)	-
0.44	10	0.962(5)	0.44(2)	0.08(2)	7.3(4)	0.23(2)	-
0.46	10	0.97(1)	0.14(2)	0.07(1)	3.2(4)	0.09(2)	-
0.50	10	0.99(1)	0.04(3)	0.06(1)	0.9(7)	0.05(3)	-
0.21	16	0.72(1)	0.65(1)	0.23(1)	4.0(1)	0.40(1)	−8.2
0.23	16	0.85(1)	0.69(1)	0.20(1)	5.0(2)	0.41(1)	-
0.25	16	0.88(1)	0.70(1)	0.194(8)	5.2(1)	0.41(1)	-
0.3	16	0.941(7)	0.71(1)	0.17(1)	6.0(2)	0.40(1)	-
0.35	16	0.966(6)	0.65(1)	0.14(1)	6.7(2)	0.35(1)	-
0.4	16	0.981(5)	0.54(2)	0.09(1)	8.6(3)	0.28(1)	-
0.44	16	0.989(4)	0.43(2)	0.064(9)	9.7(4)	0.22(2)	-

the translational long-time self-diffusion coefficient D_L^t in the *isotropic* phase [31]. Both quantities are conveniently measured in terms of the short-time limit $D^t\equiv(2D^{\perp}+D^{\parallel})/3$. The following facts can be extracted from our data.

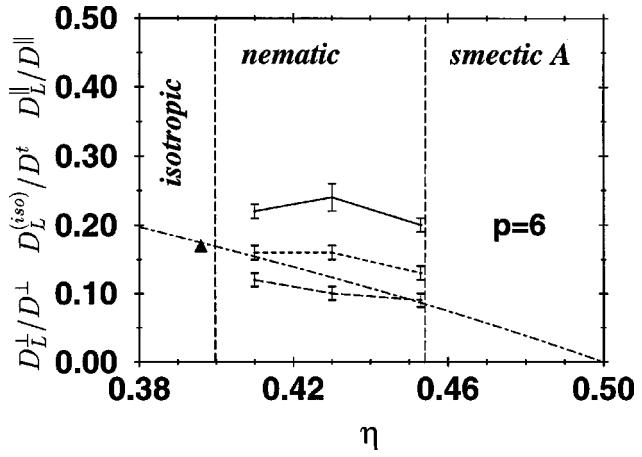

FIG. 1. The ratios $D_L^{\parallel}/D^{\parallel}$ (solid line), $D_L^{\perp}/D^{\perp}$ (long-dashed line), and $D_L^{(\mathrm{iso})}/D_0^T$ (short-dashed line) as functions of packing fraction η for fixed $p=6$. Simulation data together with their error bars are given. The lines are a guide to the eye. The long-time translational self-diffusion coefficient of the isotropic phase, measured in terms of its short-time limit at isotropic-nematic coexistence, is given by the triangle. The dot-dashed line is the long-time translational self-diffusion coefficient of the isotropic phase which is extrapolated into the nematic phase region by using the fit formula of Ref. [31]. The vertical dashed lines locate the isotropic-nematic, and the nematic–smectic-A transition.

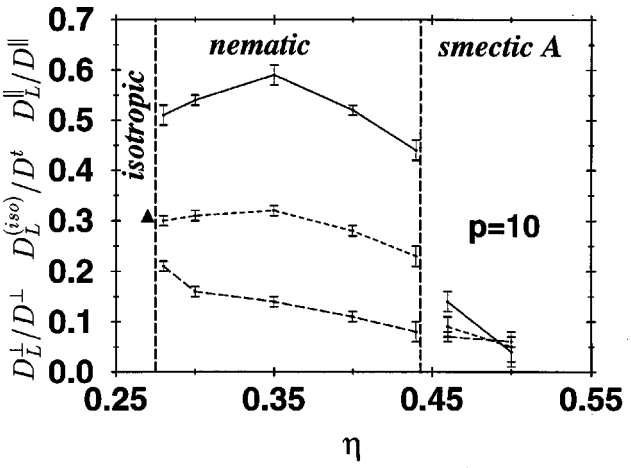

FIG. 2. Same as Fig. 1, but now for $p=10$. The results in the smectic-A phase are included.

(1) For fixed p, $D_L^{\perp}$ decreases for increasing η with an almost linear η dependence. This is similar to the isotropic case, where D_L^t also decreases with increasing packing fraction. In the fully aligned case ($S\equiv 1$), $D_L^{\perp}/D^{\perp}$ is expected to be close to the scaled long-time self-diffusion coefficient of two-dimensional Brownian disks which is well-described by $1-\frac{4}{3}\eta$ for $0\leqslant\eta\lesssim 0.7$ [26]. The actual data are much smaller than in the disc case, proving that there is a significant enhanced entanglement of nonparallel vicinal rods.

(2) The most striking fact of our data is that $D_L^{\parallel}$ behaves *nonmonotonically* with η. The diffusion along the nematic director first strongly increases, reaches a plateau, and then decreases again; see Figs. 2 and 3. There are two inverse effects competing in determining the diffusion along the director: First, the stronger alignment, as manifested by an increasing nematic order parameter S, favors lengthwise diffusion since there are less vicinal rods to cross in moving along the director. Second, with increasing η there is less free space available, which hinders diffusion in general. It is a subtle interplay between these two effects which results in the nonmonotonic behavior. Close to the isotropic-nematic transition, S rapidly changes with density. Hence diffusion along the director is accelerated with increasing density. For

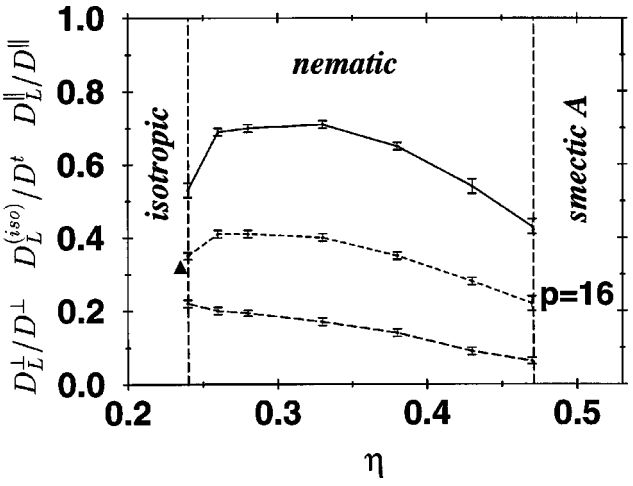

FIG. 3. Same as Fig. 1, but now for $p=16$.

higher densities, however, the alignment has practically saturated, and the packing constraints slow down any diffusion.

(3) For fixed η, $D_L^{\parallel}/D^{\parallel}$ and $D_L^{\perp}/D^{\perp}$ increase for increasing p. This fact, which can be seen by a comparison of Figs. 2 and 3, is different from the isotropic phase where D_L^t/D^t decreases for increasing p at fixed η.

(4) The ''isotropized'' diffusion $D_L^{(\mathrm{iso})}$ exhibits the same nonmonotonicity in density as $D_L^{\parallel}$: it first increases similar to earlier findings in the Yukawa-segment model [36], and then decreases again. This demonstrates that the acceleration in $D_L^{\parallel}$ is more dominant than the decrease of $D_L^{\perp}$.

Comparing the data for $D_L^{(\mathrm{iso})}/D^t$ with that for D_L^t/D^t extrapolated from the fluid phase by the fit formula given in Ref. [31], one obtains the following picture: In general, the fluid-state data for D_L^t/D^t are smaller than $D_L^{(\mathrm{iso})}/D^t$ in the nematic phase. At the isotropic-nematic transition, however, both data practically coincide. In detail, for $p=4.8$ and $\eta=0.48$, corresponding to a state point in the stability regime of the nematic phase, one has $D_L^t/D^t=0.073$, which is significantly smaller than $D_L^{(\mathrm{iso})}/D^t=0.10$. For $p=6$, isotropic-nematic coexistence is at $\eta\approx 0.41$, where $D_L^t/D^t=0.154$ practically coincides with $D_L^{(\mathrm{iso})}/D^t=0.16$. For higher densities, $\eta=0.453$ at $p=6$, one obtains a larger difference, namely, $D_L^t/D^t=0.086$ and $D_L^{(\mathrm{iso})}/D^t=0.13$. A similar trend occurs for higher aspect ratios: Here, at the isotropic-nematic transition, $D_L^t/D^t\approx 0.33$ in the isotropic phase, which is not much different from our data in the nematic phase. A similar trend was seen in the experiment of van Bruggen *et al.* [40]. The diffusion in the nematic phase, coexisting with the isotropic phase, was comparable to the diffusion extrapolated from the isotropic phase. However, in the experiment, a large density jump was observed across the isotropic-nematic transition which is different from that in our spherocylinder model, and is probably due to the more complicated effective interaction between the rods. This in turn leads to a large variation of the diffusion across the isotropic-nematic transition which does not occur in our model.

C. Ratio $D_L^{\parallel}/D_L^{\perp}$ in the nematic phase

Let us now discuss a simple *theoretical estimate* for the ratio $D_L^{\parallel}/D_L^{\perp}$. We assume that there is only motion in the direction parallel to the rod orientations. In the nematic phase, these orientations are distributed according to an orientational distribution function $g(\cos\theta)$, where θ is the angle between the rod orientation and the nematic director. The function $g(\cos\theta)$ is taken to be normalized with respect to integration over the unit sphere, such that

$$2\pi\int_0^{\pi} d\theta \sin\theta g(\cos\theta)\equiv\langle 1\rangle_g=1, \tag{17}$$

where the average $\langle\cdots\rangle_g$ is over the unit sphere involving the orientational distribution function. The associated nematic order parameter S can be expressed as an average of the second Legendre polynomial $P_2(\cos\theta)=(3\cos^2\theta-1)/2$ as

$$S=\langle P_2(\cos\theta)\rangle_g=\tfrac{3}{2}\langle\cos^2\theta\rangle_g-\tfrac{1}{2}. \tag{18}$$

Now a typical mean-square displacement parallel to the nematic director is

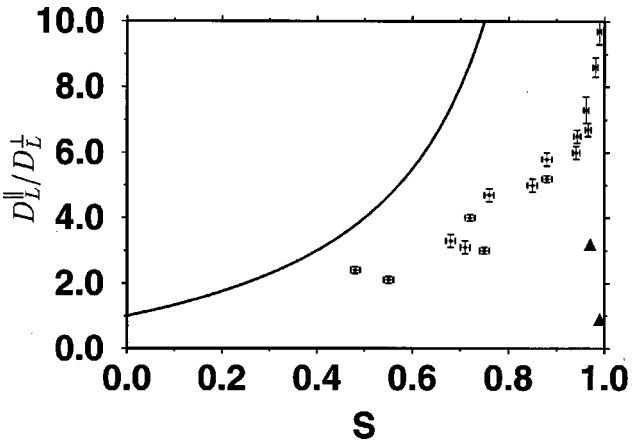

FIG. 4. Ratio of the long-time self-diffusion coefficients, $D_L^{\parallel}/D_L^{\perp}$, plotted as a function of the nematic order parameter S. The solid line is the upper bound $(2S+1)/(1-S)$. The results of the smectic A phase are given by triangles.

$$w^{\parallel}=l_0^2\langle\cos^2\theta\rangle_g, \tag{19}$$

where l_0 is a suitable length scale. Similarly,

$$w^{\perp}=l_0^2\langle\sin^2\theta\rangle_g=l_0^2(1-\langle\cos^2\theta\rangle_g)$$

is a typical mean-square displacement perpendicular to the nematic director. Consequently, $D_L^{\parallel}/D_L^{\perp}\approx 2w^{\parallel}/w^{\perp}$. Expressing this in terms of S finally yields

$$D_L^{\parallel}/D_L^{\perp}\approx\frac{2S+1}{1-S}. \tag{20}$$

Two remarks are in order: First, the right-hand-side of Eq. (20) actually should represent an *upper bound* to $D_L^{\parallel}/D_L^{\perp}$, since we neglected any parallel motion from the very beginning. Second, in this simple theoretical approach, $D_L^{\parallel}/D_L^{\perp}$ only depends on S. This is a prediction which can be tested against our simulation data. In Fig. 4, we plot our simulation results for $D_L^{\parallel}/D_L^{\perp}$ versus S. First, it can clearly be seen that the theory indeed provides an upper bound for $D_L^{\parallel}/D_L^{\perp}$. Second, the simulation data reasonably fall on a single curve showing that the essential dependence of $D_L^{\parallel}/D_L^{\perp}$ is on S alone. At the isotropic-nematic transition, the nematic order parameter grows from ≈ 0.4 to 0.784 as p increases [9]. Hence, from Fig. 3, we obtain that $D_L^{\parallel}/D_L^{\perp}$ is between 2 and 4 at the isotropic-nematic transition. This is consistent with recent experiments [40] and with simulation on the Yukawa-segment model [36].

D. Orientation flips

Finally we have calculated the rate Γ of *orientation flips* per particle in the nematic phase for relatively small densities. We define this quantity as follows: Suppose, at time zero, the actual rod orientation $\vec{\Omega}_i(0)$ is in a cone of angle $\theta_0\equiv\pi/2$ around the director $\vec{\Omega}_0$, i.e., $\vec{\Omega}_i(0)\cdot\vec{\Omega}_0>\cos\theta_0/2=1/\sqrt{2}$. Then, with a certain flip rate Γ, this orientation will be in the opposite cone after a mean time of $1/\Gamma$, i.e., $\vec{\Omega}_i(1/\Gamma)\cdot\vec{\Omega}_0<-1/\sqrt{2}$. An orientation flip is a rare event which scales with the number of particles. In the simulation

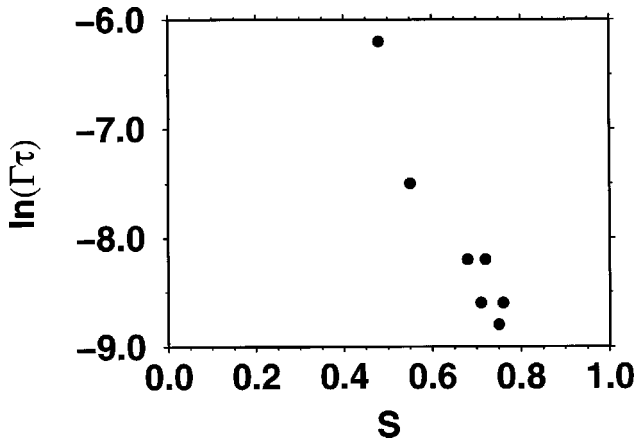

FIG. 5. Plot of the logarithm of the orientation flip rate per rod, $\ln(\Gamma\tau)$, vs the nematic order parameter S. Note that there is a large statistical error in Γ.

we average over any flip and thus extract the flip rate Γ per particle. Results for Γ are included in Table II. A plot of $\ln\Gamma$ versus S is shown in Fig. 5. Again the data reasonably fall on a single curve. However, we remark that the actual statistical error in the data for Γ is large (and could not safely be estimated), since only few events were sampled during the simulation and the boxlength in the x,y direction was not large. Also, Γ depends sensitively on the magnitude of the time step Δt. For large S, the corresponding rate was small such that no flip process at all was observed during the simulation.

E. Long-time diffusion in the smectic-*A* phase

For $p=10$, we have performed two runs in the smectic-*A* phase occurring for packing fractions $0.44<\eta<0.59$ [9]. In particular, we have chosen $\eta=0.46$ and $\eta=0.50$, see again Tables I and II and Fig. 2. While the diffusion perpendicular to the director is practically not affected by the additional smectic layering, the diffusion parallel to the director slows down dramatically due to the one-dimensional ordering. Since the nematic–smectic-*A* transition is weakly first order (i.e., the density jump across the transition is small), this slowing down is manifested only gradually across the transition. Deep in the smectic-*A* phase, however, the parallel diffusion becomes even smaller than the perpendicular diffusion, which is completely opposite to the behavior in the nematic phase. This is expected, as there is still fluidlike order perpendicular to the director which results in a significant mobility, while the increasing smectic order hinders parallel motions massively. Hence the ratio $D_L^{\parallel}/D_L^{\perp}$ *decreases* with increasing density, while it increases with increasing density in the nematic phase. In Fig. 4 the data for the smectic-*A* phase are also included, showing that they do not fall on the same universal curve as for the data in the nematic phase.

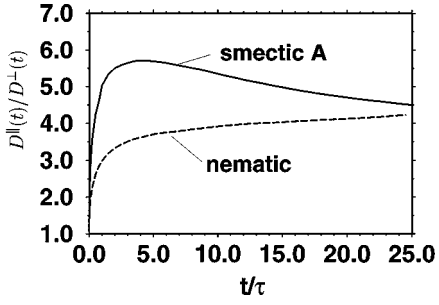

FIG. 6. The ratio $D^{\parallel}(t)/D^{\perp}(t)$ vs reduced time t/τ. The solid line is in the smectic phase with $p=10$ and $\eta=0.46$. For comparison, the monotonic behavior in the nematic phase is shown for $p=10$ and $\eta=0.3$ as a dashed curve.

A final interesting dynamical difference between the nematic and smectic-*A* phases is the time dependence of the ratio $D^{\parallel}(t)/D^{\perp}(t)$. In the nematic phase, we always found that $D^{\parallel}(t)/D^{\perp}(t)$ is increasing for increasing time t. This is different in the smectic phase, where $D^{\parallel}(t)/D^{\perp}(t)$ is nonmonotonic in time; see Fig. 6. For small times, $D^{\parallel}(t)/D^{\perp}(t)$ starts from values close to $D^{\parallel}/D^{\perp}$, which is the limit of fully aligned rods. Then, for short times, the parallel motion is faster than the perpendicular one, since the rods experience fluctuations and undulations of the smectic layers. Then, after an intermediate time, $D^{\parallel}(t)/D^{\perp}(t)$ reaches a maximum and decreases, as the rods now realize the one-dimensional confinement parallel to the director. The long-time parallel diffusion is dominated by hopping processes between vicinal smectic layers.

V. CONCLUSIONS

Using Brownian dynamics simulations of colloidal hard spherocylinders, we have calculated the anisotropic translational long-time self-diffusion coefficients in the nematic phase. The diffusion along the director was nonmonotonic with density. The ratio $D_L^{\parallel}/D_L^{\perp}$ was about 2–4 near the isotropic-nematic transition, and is increasing for increasing density. Both $D_L^{\parallel}/D_L^{\perp}$ and the orientation flip rate depend mainly on the nematic order parameter S. In the smectic-*A* phase, the picture was different: Here, the diffusion along the director drops down rapidly, even below the perpendicular diffusion, such that $D_L^{\parallel}/D_L^{\perp}$ decreases for increasing density. We end with several comments related to future problems and experiments.

(i) First, a low-density expansion for the long-time self-diffusion coefficients was recently successfully accomplished by Dhont, van Bruggen, and Briefs [46] in the isotropic phase using a variational approach. It would be interesting to extend this theory to the nematic phase and to compare with our simulational data.

(ii) The long-time tail corrections to $D^{\parallel}(t)$ and $D^{\perp}(t)$ are only known for spheres [24] but not for rods. It would be interesting to do an analysis for rodlike particles in the isotropic, nematic, and smectic phases.

(iii) A comparison with experimental colloidal samples may be spoiled by the intrinsic polydispersity of the rods. Nevertheless, it should be possible to perform measurements on samples similar to that used in Ref. [37] in the nematic and smectic phases. Thus an experimental verification of our theoretical predictions is possible, at least in principle. It would be interesting to verify the nonmonotonic behavior of the long-time self-diffusion along the nematic director experimentally by using more concentrated nematic samples than that used in Ref. [40].

(iv) The present study is for prolate objects. No Brownian

dynamics simulations were performed for oblate particles such as, e.g., clay platelets. The phase diagram of hard ellipsoids of revolution exhibits a remarkable symmetry between prolate and oblate shapes [47]. Therefore it would be interesting to check whether a similar scenario for the long-time quantities is valid across the isotropic-nematic transition for platelets. What one expects here, is that the diffusion along the nematic director is smaller than the perpendicular diffusion.

ACKNOWLEDGMENTS

The author thanks J. K. G. Dhont, A. Jusufi, and H. Graf for helpful discussions.

[1] L. Onsager, Ann. (N.Y.) Acad. Sci. **51**, 627 (1949).
[2] For a review, see M. P. Allen, G. T. Evans, D. Frenkel, and B. M. Mulder, in *Advances in Chemical Physics*, edited by I. Prigogine and S. A. Rice (Wiley, New York, 1993), Vol. LXXXVI, p. 1.
[3] E. Canessa, B. D'Aguanno, B. Weyerich, and R. Klein, Mol. Phys. **73**, 175 (1991).
[4] S.-D. Lee, J. Chem. Phys. **87**, 4972 (1987).
[5] A. Poniewierski and R. Holyst, Phys. Rev. Lett. **61**, 2461 (1988); Phys. Rev. A **41**, 6871 (1990).
[6] J. Herzfeld, Acc. Chem. Res. **29**, 31 (1996); J. Han and J. Herzfeld, in MRS Symposia Proceedings No. 436 (Materials Research Society, Pittsburgh, 1997), p. 135.
[7] M. F. Sharlow, R. L. B. Seliger, A. Ben-Shaul, and W. M. Gelbart, J. Phys. Chem. **99**, 2907 (1995).
[8] J. A. C. Veerman and D. Frenkel, Phys. Rev. A **41**, 3237 (1990).
[9] P. G. Bolhuis and D. Frenkel, J. Chem. Phys. **106**, 666 (1997).
[10] H. Graf, H. Löwen, and M. Schmidt, Prog. Colloid Polym. Sci. **104**, 177 (1997).
[11] P. G. Bolhuis, A. Stroobants, D. Frenkel, and H. N. W. Lekkerkerker, J. Chem. Phys. **107**, 1551 (1997).
[12] P. van der Schoot, J. Phys. II **6**, 1557 (1996).
[13] S. B. Chen and D. L. Koch, J. Chem. Phys. **104**, 359 (1996).
[14] J. M. Deutsch and N. Goldenfeld, J. Phys. (France) **43**, 631 (1982); T. Sato and A. Teramoto, Physica A **176**, 72 (1991).
[15] H. Graf and H. Löwen, Phys. Rev. E (to be published).
[16] A. Yethiraj and H. Fynewever, Mol. Phys. **93**, 693 (1998).
[17] For a review, see G. J. Vroege and H. N. W. Lekkerkerker, Rep. Prog. Phys. **55**, 1241 (1992); H. N. W. Lekkerkerker, P. Buining, J. Buitenhuis, G. J. Vroege, and A. Stroobants, in *Observation, Prediction and Simulation of Phase Transitions in Complex Fluids*, Vol. 460 of *NATO Advanced Study Institute Series C: Mathematical and Physical Sciences*, edited by M. Baus, L. F. Rull, and J. P. Ryckaert (Kluwer, Dordrecht, 1995), pp. 53–112.
[18] S. Fraden, in *Observation, Prediction and Simulation of Phase Transitions in Complex Fluids* (Refs. [17]), pp 113–164.
[19] P. A. Buining, A. P. Philipse, and H. N. W. Lekkerkerker, Langmuir **10**, 2106 (1994).
[20] J. K. G. Dhont, *An Introduction to Dynamics of Colloids* (Elsevier, Amsterdam, 1996).
[21] G. Nägele, T. Zwick, R. Krause, and R. Klein, J. Colloid Interface Sci. **161**, 347 (1993).
[22] H. Löwen, J.-P. Hansen, and J. N. Roux, Phys. Rev. A **44**, 1169 (1991).
[23] W. van Megen and I. Snook, J. Chem. Soc., Faraday Trans. **80**, 383 (1984).
[24] B. Cichocki and K. Hinsen, Physica A **166**, 473 (1990); **187**, 133 (1992).
[25] W. Schaertl and H. Sillescu, J. Colloid Interface Sci. **155**, 313 (1993).
[26] H. Löwen and G. Szamel, J. Phys.: Condens. Matter **5**, 2295 (1993).
[27] H. Löwen, T. Palberg, and R. Simon, Phys. Rev. Lett. **70**, 1557 (1993); F. Bitzer, T. Palberg, H. Löwen, R. Simon, and P. Leiderer, Phys. Rev. E **50**, 2821 (1994).
[28] A. V. Indrani and S. Ramaswamy, Phys. Rev. Lett. **73**, 360 (1994); **74**, 1491 (1995); M. Fuchs, *ibid.* **74**, 1490 (1995).
[29] P. Espanol and I. Zuniga, Int. J. Mod. Phys. B **9**, 469 (1995).
[30] H. Löwen, Phys. Rev. E **53**, R29 (1996).
[31] H. Löwen, Phys. Rev. E **50**, 1232 (1994).
[32] A. C. Branka and D. M. Heyes, Phys. Rev. E **50**, 4810 (1994).
[33] D. M. Heyes and P. J. Mitchell, J. Phys.: Condens. Matter **6**, 6423 (1994); J. Chem. Soc., Faraday Trans. **90**, 1931 (1994); A. C. Branka and D. M. Heyes, J. Chem. Phys. **109**, 312 (1998).
[34] I. Bitsanis, H. T. Davis, and M. Tirrell, Macromolecules **21**, 2824 (1988); **23**, 1157 (1990).
[35] L. Johansson and J. E. Löfroth, J. Chem. Phys. **98**, 7471 (1993).
[36] T. Kirchhoff, H. Löwen, and R. Klein, Phys. Rev. E **53**, 5011 (1996).
[37] M. P. B. van Bruggen, H. N. W. Lekkerkerker, and J. K. G. Dhont, Phys. Rev. E **56**, 4394 (1997).
[38] M. P. B. van Bruggen, Langmuir **14**, 2245 (1998).
[39] Z. Bu, P. S. Russo, D. L. Tipton, and I. I. Negulesco, Macromolecules **27**, 6871 (1994).
[40] M. P. B. van Bruggen, H. N. W. Lekkerkerker, G. Maret, and J. K. G. Dhont (unpublished).
[41] Note that in Refs. [8,9] L does not denote the total rod length but that of the cylindric part. Correspondingly the aspect ratio p differs from our definition by 1.
[42] S. Broersma, J. Chem. Phys. **32**, 1626 (1960); **32**, 1632 (1960); **74**, 6989 (1981).
[43] M. M. Tirado and J. G. de la Torre, J. Chem. Phys. **71**, 2581 (1979); **73**, 1986 (1980).
[44] M. M. Tirado, C. L. Martinez, and J. G. de la Torre, J. Chem. Phys. **81**, 2047 (1984).
[45] S. Fraden, G. Maret, D. L. D. Caspar, and R. B. Meyer, Phys. Rev. Lett. **63**, 2068 (1989); X. Wen, R. B. Meyer, and D. L. D. Caspar, *ibid.* **63**, 2760 (1989).
[46] J. K. G. Dhont, M. P. B. van Bruggen, and W. J. Briels (private communication).
[47] D. Frenkel and B. M. Mulder, Mol. Phys. **55**, 1171 (1985).